Unbalanced Voltage Suppression of Bipolar DC Microgrids with Integration of DC Zero-carbon Buildings

Xuefei Zhang, Chunsheng Guo, Yiyao Zhou, Xiaolong Xu, Jianquan Liao, Niancheng Zhou, and Qianggang Wang

***Abstract*—Considering the majority of electrical equipment utilized in society is driven by DC, integrating a DC system can significantly enhance the efficiency and reliability of power systems by implementing the integration of diverse loads, renewable energy sources (RESs), and energy storage systems (ESSs). In this paper, the integration of multiple DC zero-carbon buildings (DC-ZCBs) is proposed to achieve the unbalanced voltage suppression of the bipolar DC microgrid (DCMG). The photovoltaic (PV) technology, loads, and DC electric springs (DC-ESs) are adopted as a unified entity to achieve the zero-carbon emission of the building. Firstly, a new configuration of PV and DC-ESs is introduced. The energy management of PV, ESS, and load are fully considered in this new configuration, which can reduce the capacity of the ESS. Subsequently, a distributed cooperative control strategy for DC-ESs based on the modulus voltage is presented, which is implemented with integration of the new configuration into the bipolar DCMG. The proposed approach addresses the issues of unbalanced voltage to improve the operating efficiency and power quality of the bipolar DCMG. The simulation is conducted in MATLAB/Simulink platform to confirm the effectiveness of the proposed approach.**

***Index Terms*—Bipolar DC microgrid (DCMG), DC zero-carbon building (DC-ZCB), electric spring (ES), modulus voltage control, unbalanced voltage suppression.**

I. Introduction

CURRENTLY, AC microgrid (ACMG) dominates the market for power distribution and transmission [1], [2]. However, ACMGs suffer from several drawbacks such as the inability to connect DC loads directly, the need for additional power conversion stages leading to the increase of power losses, difficulties in frequency and phase synchronization [3]-[5], and environmental concerns [6]. Therefore, the adoption of a bipolar DC microgrid (DCMG), which utilizes the distributed renewable energy source (RES) such as photovoltaic (PV), is becoming more efficient and reliable.

Most of the bipolar DCMGs are low-carbon systems consisting of loads, RESs, and energy storage systems (ESSs). The DC building can function as load or contribute to voltage regulation in the bipolar DCMG when combined with ESSs [7]. The DC zero-carbon building (DC-ZCB) is a component of a broader energy system aimed at achieving overall carbon neutrality [8], [9]. The availability of the affordable and effective DC/DC converters is also contributed to the prosperity of DC-ZCBs. Recent studies show that the bipolar DCMG with the integration of DC-ZCBs can significantly benefit from technological advancements in power generation, transmission, distribution, storage, and control [1]. The present configuration of bipolar DCMG with the integration of DC-ZCBs can be classified into unipolar and bipolar DCMGs based on the number of DC buses [10]. The bipolar DCMG with the integration of DC-ZCBs has the advantage of the additional neutral bus, providing the following benefits.

1) Providing more voltage levels with fewer buses, minimizing power conversion, and boosting overall efficiency [11], [12].

2) Enhancing the utilization of DC-ZCBs in bipolar DCMG with integration of RESs, ZCBs, and electric vehicle charging facilities [13].

3) Enhancing stability with a three-wire structure ensures that if one of the DC buses fails, the remaining buses will continue to operate normally [14].

Although the bipolar DCMG with the integration of DC-ZCBs has advantages, the issue of the unbalanced voltage must be addressed [8]. The unbalanced voltage in the bipolar DCMG can result in voltage and current disturbances, which further increase power losses and haste device aging [15], [16]. Hence, it is crucial to employ suitable approaches to suppress the unbalanced voltage in the bipolar DCMG.

According to the existing studies, achieving the optimization of the bipolar DCMG voltage primarily involves utilizing flexible electronic equipment or a new control topology.

One approach to addressing the issue of unbalanced volt-

Manuscript received: September 27, 2023; revised: Febuary 6, 2024; accepted: April 2, 2024. Date of CrossCheck: April 2, 2024. Date of online publication: April 23, 2024.

This work was supported by the National Natural Science Foundation of China (No. 52077017).

X. Zhang, Y. Zhou, X. Xu, N. Zhou, and Q. Wang are with the State Key Laboratory of Power Transmission Equipment Technology, School of Electrical Engineering, Chongqing University, Chongqing, China (e-mail: zhangxuefei@cqu.edu.cn; yiyaozhou@cqu.edu.cn; xuxiaolong@cqu.edu.cn; cee_nczhou@cqu.edu.cn; qianggang1987@cqu.edu.cn).

C. Guo and J. Liao (corresponding author) are with the College of Electrical Engineering, Sichuan University, Chengdu, China (e-mail: jquanliao@scu.edu.cn; kiritodile@outlook.com).

DOI: 10.35833/MPCE.2023.000713

age is to utilize flexible electronic equipment. Reference [17] introduces a voltage balancer (VB) with the capability of a DC/DC converter. However, the VB has limitations, as the output power is always lower than the unbalanced power, making it difficult to respond to the changes in DC load. In the case of multiple VBs, the control between different VBs and rectifiers must be coordinated [18], [19], which is complicated with multiple power supplies [20], [21]. Furthermore, when the distribution line is long and has many load nodes, this coordination control may not guarantee the voltage of the constant power load (CPL) at the end of the distribution line. An alternative approach is the consensus control system based VB proposed in [22], in which the primary and secondary controls are both integrated in bipolar DCMG. However, the consensus control system requires a spare communication system to facilitate information sharing among multiple nodes, which increases the cost and complexity of the power network. Another approach is introduced in [23], which involves using a DC electric spring (DC-ES) to regulate the voltage disturbance on the load side in the bipolar DCMG. Thus, the proposed approach in [23] enhances the dynamic performance of the control system by building a transfer matrix that adopts the DC-ES decoupling control. However, in engineering applications, the recommended approaches are both costly and complex.

Another approach to address the issue of unbalanced voltage involves adopting a new control topology. Novel power sharing strategies and voltage regulation approaches are proposed in [18], [19], [24], and [25]. However, they cannot solve communication burden problems. In [26]-[29], power sharing and energy management approaches for DCMGs are proposed. However, they have not investigated the effect of PV system characteristics on the control strategies with high PV penetration in bipolar DCMG. Therefore, these approaches are not applicable to the unbalanced voltage suppression in DCMGs with the integration of ZCBs. Additionally, the above-mentioned approaches require communication systems during the control process. It is possible to employ the modulus voltage control to reduce the unbalanced voltage brought by droop control [13], [30], and [31]. Consequently, the unbalanced voltage issue in the bipolar DCMG needs more consideration. However, those studies have not investigated the impact of coupled parameters on stability. When the distribution lines are coupled in the bipolar DCMG, the challenge of setting control parameters can be resolved through the proposed approach in this paper. The proposed approach, which compensates for the voltage drop in the neutral line and enhances the dynamic performance of the control system.

In bipolar DCMGs with the integration of ZCBs including PV, the increasing PV penetration makes it challenging to accommodate its generation. Moreover, the stochastic and fluctuating nature of PV poses higher challenges to the unbalanced voltage suppression in bipolar DCMGs. This paper addresses the impact of high PV penetration in the DCMG with the integration of PV and DC-ES. Additionally, a modulus voltage consensus control approach is proposed to precisely suppress the unbalance voltage while simplifying the complexity of the unbalanced voltage control system. A comparison with [24] and [32] shows that the proposed approach in this paper successfully decouples the coupling between the two poles of the power supply and the bipolar control system, effectively suppressing the unbalanced parameters. The main contributions of this paper can be summarized as follows.

1) The integration of PV and DC-ES reduces the volume and weight of the ESS in DC-ES. This integration mitigates the randomness and volatility of PV, enhancing the renewable energy absorption capability of the DC-ZCB.

2) The modular transformation is introduced, which decouples bipolar DCMGs interconnected through the neutral line resistance. This simplifies control objectives and reduces the control complexity to facilitate coordinated control among multiple devices.

3) A distributed cooperative control strategy is proposed for PV-DC-ES in bipolar DCMGs for unbalanced voltage suppression, which not only enhances the electric power quality of bipolar DCMGs but also reduces system losses.

The rest of this paper is organized as follows. Section II presents the analysis of DC-ES in bilopar DCMG with integration of DC-ZCBs. Section III details the distributed cooperative control strategy. Section IV investigates the consistency in control performance and small-signal stability analysis. Section V presents the simulation results. Finally, Section VI gives the conclusion of this paper.

II. Analysis of DC-ES in Bipolar DCMG with Integration of DC-ZCBs

A. Type, Topology, and Working Mode of DC-ES

DC-ES can be widely distributed at any node of the DCMG. When there are non-critical loads (NCLs) with a broad voltage range, a smart load may be created by connecting DC-ES in series or parallel to ensure the voltage stability of critical loads (CLs). Depending on the installation position of the NCL, DC-ES may be classified into series DC-ES and parallel DC-ES. The basic structures of different types of DC-ES are shown in Fig. 1, where V_{PCC} is the common-node voltage; R_C is the equivalent resistance of CL; R_{NC} is the equivalent resistance of NCL; R_L is the line resistance; V_s is the equivalent voltage on the source side of the bipolar DCMG; and V_{es} is the output equivalent voltage of DC-ES. According to [33] and [34], the working modes of series DC-ES are divided into boost discharging, boost charging, and depressing discharging.

The structure of bipolar DCMG with the integration of DC-ZCBs is shown in Fig. 2. The loads in the DC-ZCBs are divided into CLs and NCLs, which make up around 46% and 54% of the total loads in the DC-ZCBs, respectively [35]. CLs mainly include office equipment, intelligent control equipment, etc. NCLs mainly include light loads, cooling loads, and heat loads, e. g., air conditioners and water heaters. Since CLs are sensitive to voltage quality, it is important to ensure that the voltage under the DC voltage state with little fluctuation at both ends of the load. NCLs may

function in a wide voltage range and have minimal voltage quality requirements.

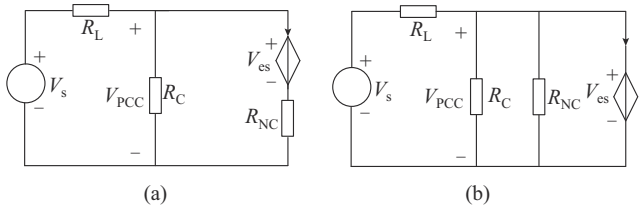

Fig. 1. Basic structure of different types of DC-ES. (a) Series DC-ES. (b) Parallel DC-ES.

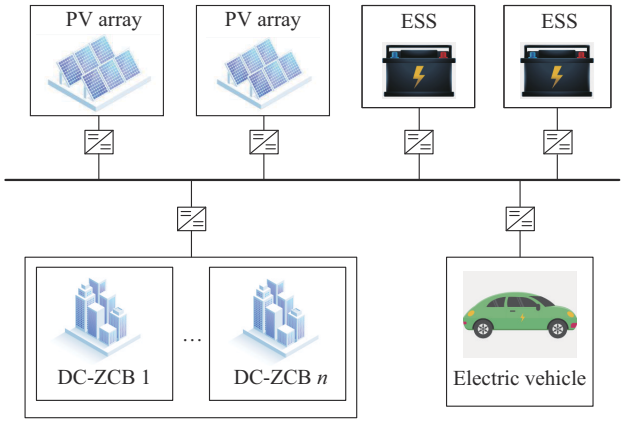

Fig. 2. Structure of bipolar DCMG with integration of DC-ZCBs.

The composition of power supply and load in bipolar DCMG with the integration of DC-ZCBs is shown in Fig. 3. According to Fig. 3, the response capability of demand side for NCLs is not completely utilized since both CLs and NCLs are linked in parallel with the DC bus [35]. For instance, NCLs are unable to actively reduce their own power in response to PV power fluctuations when ESS and PV power are both inadequate.

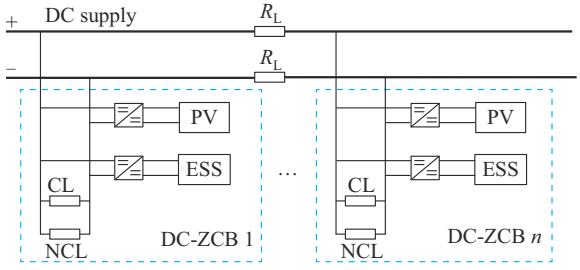

Fig. 3. Composition of power supply and load in bipolar DCMG with integration of DC-ZCBs.

To fully exploit the demand-side response capability of NCLs, both CLs and NCLs in DC-ZCB can be reconfigured. At the same time, the installation position of PV can be reconfigured. Reference [35] proposes a novel concept of PV-embedded DC-ES by transferring a portion of PV panels from the grid to the DC link of the DC-ES. As the output power is no longer solely derived from the energy storage device, The size and volume of ESS can be significantly reduced. In order to create a smart load, the DC converter of ESS is coupled with NCLs. This structure can adjust the power of NCLs in real time according to the bus voltage. The bipolar DCMG with the integration of DC-ZCBs contains the PV power generation system and ESS, which can supply power to the loads, as illustrated in Fig. 4(a). In addition, part of the PV connected to the DC bus is embedded into DC-ES to form a PV-DC-ES structure, as illustrated in Fig. 4(b). The bipolar DCMG coupled with DC-ZCBs can drastically lower the capacity and volume of the ESS because the output power of the DC-ES is no longer completely derived from the ESS.

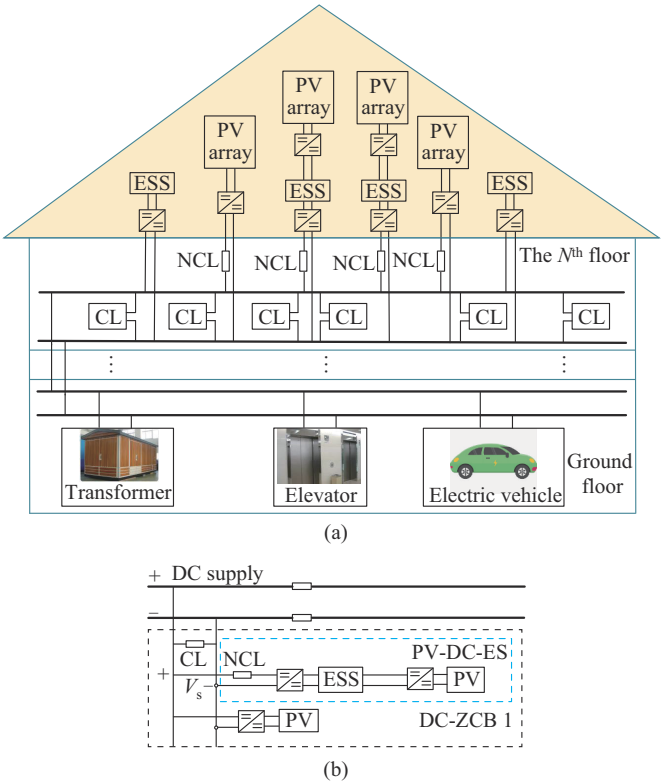

Fig. 4. Structure of DC-ZCBs and PV-DC-ES. (a) Structure of DC-ZCBs with power supply and load. (b) Structure of PV-DC-ES in bipolar DCMG with integration of DC-ZCBs.

DC-ZCB with the integration of PV-DC-ES in a bipolar DCMG shows a significant promise in reducing the capacity and volume requirements of the ESS. This is attributed to the fact that the output power of the DC-ES is no longer solely dependent on the ESS. Future studies on DC-ZCB with the integration of PV-DC-ES can explore several key aspects. Firstly, the integration represents a key step towards sustainable and efficient energy solutions [34], [36], [37]. Optimizing DC-ZCB with the integration of PV-DC-ES stands as a potential avenue for enhancing system efficiency, maximizing overall energy yield, and minimizing losses during energy conversion and energy storage processes. Secondly, DC-ZCB with the integration of PV-DC-ES brings several advantages concerning DCMG integration and resilience [38]. The PV-DC-ES can contribute to grid-friendly functionalities, explore DCMG applications, and strengthen the system resilience against fluctuations and disturbances. Lastly, PV-DC-ES with the integration of smart building technolo-

gies holds the potential to augment overall functionality and energy management capabilities.

In this paper, the PV-DC-ES is implemented as the fundamental unit to analyze the coordinated control performance under bus voltage disturbances. Subsequently, a distributed cooperative control strategy based on modulus voltage for PV-DC-ES unit is presented. Figure 5 depicts the structure of PV-DC-ES in bipolar DCMG with the integration of DC-ZCBs, where +, −, and 0 are the positive, negative, and neutral lines, respectively; and R_{pi} and R_{ni} are the resistances of equivalent positive and negative loads at node i, respectively. Since the control goal of PV-DC-ES is to maintain the voltage of the DC link at a constant level, PV-DC-ES is equivalent to a DC power supply under steady-state conditions. Because of the differences in the capacity and operating conditions of different PV-DC-ESs, each PV-DC-ES needs to adaptively suppress the disturbance in accordance with its own capabilities when there is a disturbance in the DC bus. Due to the interdependence between the two poles of the bipolar DCMG, control actions on one pole will have an impact on the other. This paper proposes a distributed cooperative control strategy based on the idea of modulus transformation, which enables independent adjustment of the two poles. When this approach is applied, the bipolar DCMG is equivalently operated as two unipolar DCMGs.

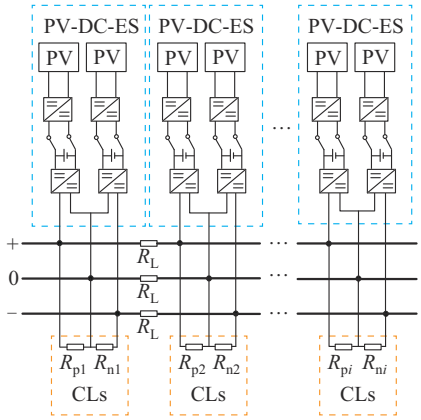

Fig. 5. Structure of PV-DC-ES in bipolar DCMG with integration of DC-ZCBs.

Figure 6 shows the structure of two-node equivalent circuit of bipolar DCMG with integration of DC-ZCBs and DC-ES. In this circuit, V_{spi} and V_{sni} are the positive and negative output voltages of node i, respectively; and I_p, I_m, and I_n are the currents on the positive line, neutral line, and negative line, respectively. For ease of investigation, it is assumed that all the equivalent line resistances are identical. As shown in Fig. 6, the two-node equivalent circuit also incorporates a neutral resistance, implying that the bipolar DCMG with the integration of DC-ZCBs and DC-ES cannot be perceived as two disparate unipolar systems.

According to Thevenin's theorem and the equivalent model in Fig. 6, it can be known that Kirchhoff's voltage law meets:

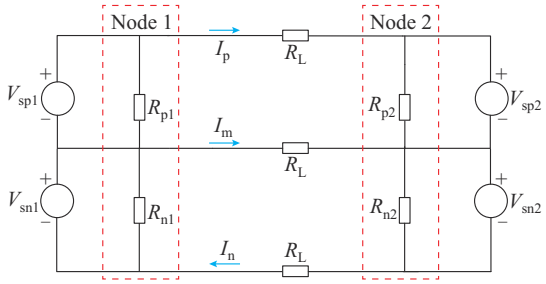

Fig. 6. Structure of two-node equivalent circuit of bipolar DCMG with integration of DC-ZCBs and DC-ES.

$$\begin{cases} -V_{sp1} - I_p R_L + V_{sp2} - I_m R_L = 0 \\ -V_{sn1} + I_m R_L + V_{sn2} + I_n R_L = 0 \\ I_m = I_n - I_p \end{cases} \tag{1}$$

The expression of line currents can be obtained by solving (1).

$$\begin{cases} I_p = \dfrac{2V_{sp1} + V_{sn1} - (2V_{sp2} + V_{sn2})}{3R_L} \\ I_n = \dfrac{2V_{sn1} + V_{sp1} - (2V_{sn2} + V_{sp2})}{3R_L} \\ I_m = \dfrac{V_{sp1} - V_{sp2} + V_{sn2} - V_{sn1}}{3R_L} \end{cases} \tag{2}$$

The positive and negative DC-ESs interact during current distribution, hindering independent control and complicating controller design. In [31], the modulus decomposition is introduced to exclude the coupling issues between the positive and negative poles. This facilitates the design for the controller as the common-mode circuit and differential-mode circuit are decoupled from each other. The transformation equation for modulus components is given in [32], [39] as:

$$\begin{bmatrix} X_0 \\ X_1 \end{bmatrix} = \boldsymbol{T} \begin{bmatrix} X_p \\ X_n \end{bmatrix} = \frac{1}{2} \begin{bmatrix} 1 & 1 \\ 1 & -1 \end{bmatrix} \begin{bmatrix} X_p \\ X_n \end{bmatrix} \tag{3}$$

where X is the voltage or current in the power system; $\boldsymbol{T}$ is the transformation matrix; the subscripts "0" and "1" represent the common-mode component and differential-mode component, respectively; and subscripts "p" and "n" represent the positive pole and the negative pole in the power system, respectively.

In (3), the pole voltages of node 1 and node 2 can be transformed into common-mode components V_{01} and V_{02}, respectively. The calculation formulas are given as:

$$\begin{cases} V_{01} = \dfrac{V_{sp1} - V_{sn1}}{2} \\ V_{02} = \dfrac{V_{sp2} - V_{sn2}}{2} \\ V_{11} = \dfrac{V_{sp1} + V_{sn1}}{2} \\ V_{12} = \dfrac{V_{sp2} + V_{sn2}}{2} \end{cases} \tag{4}$$

where V_{11} and V_{12} are the differential-mode components of V_{01} and V_{02}, respectively.

Substituting (4) into (2) yields:

$$\begin{cases} I_{\mathrm{p}} = \dfrac{V_{\mathrm{sp1}} - V_{\mathrm{sp2}} + 2(V_{01} - V_{02})}{3R_{\mathrm{L}}} \\ I_{\mathrm{n}} = \dfrac{V_{\mathrm{sn1}} - V_{\mathrm{sn2}} + 2(V_{01} - V_{02})}{3R_{\mathrm{L}}} \\ I_{\mathrm{m}} = \dfrac{2(V_{01} - V_{02})}{3R_{\mathrm{L}}} \end{cases} \tag{5}$$

According to (5), the line currents are correlated with the voltage difference between two nodes and the difference in common-mode voltage. When $V_{01} = V_{02}$, the line current meets the requirements:

$$\begin{cases} I_{\mathrm{p}} = \dfrac{V_{\mathrm{sp1}} - V_{\mathrm{sp2}}}{R_{\mathrm{L}}} \\ I_{\mathrm{n}} = \dfrac{V_{\mathrm{sn1}} - V_{\mathrm{sn2}}}{R_{\mathrm{L}}} \\ I_{\mathrm{m}} = 0 \end{cases} \tag{6}$$

According to (4) and (6), when $V_{01} = V_{02}$, I_{p} is only determined by the positive output voltage and is independent of the negative output voltage. I_{n} also comes to the same conclusion. In addition, the neutral current is 0, which can minimize the line loss of the bipolar DCMG.

B. Influence of DC-ES Output Voltage on Current

Figure 7 shows the changes of line currents under different V_{sp1}. The parameters of bipolar DCMG are detailed in Table I. As can be observed from Fig. 7(a), when V_{sp1} changes, I_{p} changes from –100 A to 166.7 A, I_{n} changes from –50 A to 83.3 A, and I_{m} is not equal to 0, the change of which is contrary to the change of I_{n}. The changing trend of Fig. 7(b) is the same as that of Fig. 7(a) and the intersection point of current changes accordingly.

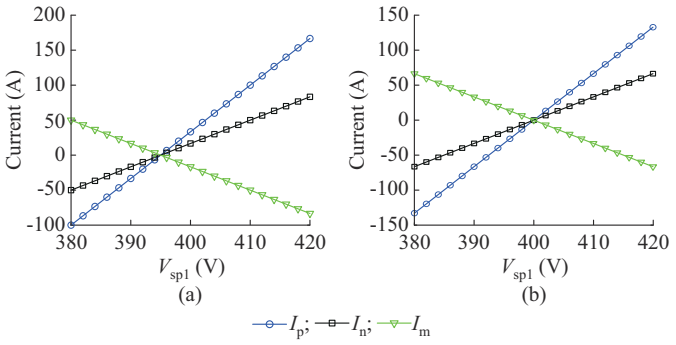

Fig. 7. Changes of line currents under different V_{sp1}. (a) $V_{\mathrm{sn2}} = V_{\mathrm{sp2}} = 395$ V. (b) $V_{\mathrm{sn2}} = 400$ V and $V_{\mathrm{sp2}} = 395$ V.

TABLE I
PARAMETERS OF BIPOLAR DCMG

Parameter	Value
V_{sn1}	400 V
R_{p1}	10 Ω
R_{n1}	20 Ω
R_{L}	0.1 Ω
R_{p2}	20 Ω
R_{n2}	20 Ω

When the proposed strategy is adopted to guarantee that the common-mode voltages of two nodes are the same, the voltage deviation can be reduced, and the voltage drop is offset on the neutral line. The related parameters are provided below to examine the impact of the changing V_{sp1} on unbalanced voltage coefficient and voltage deviation in Fig. 6, which presents the structure of bipolar DCMG. The definition of unbalanced voltage coefficient ε_{u} is given as:

$$\varepsilon_{\mathrm{u}} = \frac{v_{\mathrm{p}} - v_{\mathrm{n}}}{\dfrac{v_{\mathrm{p}} + v_{\mathrm{n}}}{2}} \times 100\% \tag{7}$$

where v_{p} and v_{n} are the positive voltage and negative voltage, respectively.

It is crucial to note that an excessively high unbalanced voltage coefficient ε_{u} can lead to the increase of power losses in the system and, in severe cases, impact the normal operation of the load. As there are currently no standardized quality criteria for DC power systems, we have adopted the unbalanced voltage coefficient from AC power systems as an indicator. In accordance with ANSI C84 standards, restricting the unbalanced voltage coefficient within 3% ensures the steady-state condition of the power system [23]. Figure 8 shows the changes of neutral line current and unbalanced voltage coefficient under different V_{sp1}. Specifically, when V_{sp1} changes, the relationship between neutral line current and the voltage is unbalanced at Node 1. As illustrated in Fig. 2, the trend of variation in neutral line current is opposite to the trend of unbalanced voltage. When the neutral line current is equal to 0, the unbalanced voltage is also equal to 0.

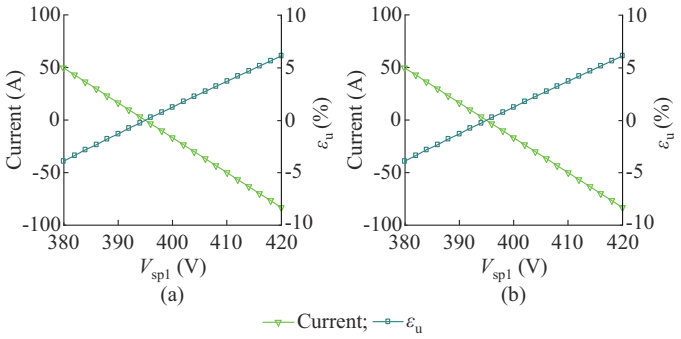

Fig. 8. Changes of neutral line current and unbalanced voltage coefficient ε_{u} under different V_{sp1}. (a) $V_{\mathrm{sn2}} = V_{\mathrm{sp2}} = 395$ V. (b) $V_{\mathrm{sp2}} = 400$ V and $V_{\mathrm{sn2}} = 395$ V.

Figure 9(a) illustrates the changes of line current with V_{sp1} when $R_{\mathrm{L}} = 0.1$ Ω and $V_{\mathrm{sp2}} = V_{\mathrm{sn2}} = 400$ V. V_{sp1} varies from 380 V to 420 V. In Fig. 9(b), $V_{\mathrm{sp2}} = 395$ V and $V_{\mathrm{sn2}} = 400$ V, and the rest of parameters match those in Fig. 9(a). According to Fig. 9(a), when $V_{\mathrm{sp2}} = V_{\mathrm{sn2}}$, V_{sp1} and V_{sn1} change synchronously. Therefore, I_{p} and I_{n} are always equal while I_{m} is always equal to 0. According to Fig. 9(b), the changing trends of I_{p} and I_{n} are the same. Since V_{sp2} and V_{sn2} are not equal, it can be obtained that $I_{\mathrm{p}} \neq I_{\mathrm{n}}$ and $I_{\mathrm{m}} \neq 0$. Therefore, it can be inferred that when there is a voltage deviation between the positive and negative nodes, I_{m} is not equal to 0,

which is the primary cause of rising network loss and coupling the issues between positive and negative poles.

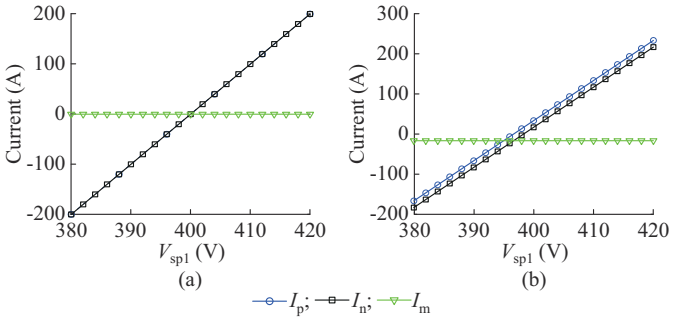

Fig. 9. Changes of line currents under different V_{sp1}. (a) $V_{sp2}=V_{sn2}=400$ V. (b) $V_{sp2}=395$ V and $V_{sn2}=400$ V.

III. Distributed Cooperative Control in Bipolar DCMG with Integration of DC-ZCBs

The proposed strategy in this paper can be explained and analyzed from two perspectives: multi-device (i. e., PV-DC-ES) coordination control and modular decoupling of the DC-MG. This paper employs distributed cooperative control strategy involving common-mode and differential-mode operations within a control loop decoupled by modulus, simplifying control objectives and reducing control complexity to facilitate coordinated control among multiple devices. The proposed strategy based on modulus voltage consensus control to coordinate the DC-ESs in each node of the bipolar DC-MG for unbalanced voltage suppression while simultaneously ensuring voltage consistency of all nodes.

A. Combination of Traditional Voltage Control and Modulus Voltage Control

The investigation in Section II indicates that the characteristic of voltage droop in the bipolar DCMG with the integration of ZCBs can be represented as a droop surface that is dependent on both polar and neutral currents. To incorporate this characteristic into the control system of the bipolar DC-MG, traditional voltage control is designed based on (1) and (2), as shown in Fig. 10, where v_{pi} and v_{ni} are the voltage outputs of the positive and negative poles of the distributed generation (DG) at node i, respectively; i_{pi} and i_{ni} are the positive and negative output currents at node i, respectively; v_{0i} and v_{1i} are the the transformed common-mode and differential-mode voltages at node i, respectively; i_{0i} and i_{1i} are the transformed common-mode and differential-mode currents at node i, respectively; $v_{0\text{ref}}$ and $v_{1\text{ref}}$ are the reference values of common-mode and differential-mode voltages, respectively; R_0 and R_1 are the common-mode and differential-mode droop resistance, respectively; K_p and K_i are the proportional and integral control ratios, respectively; d_{0i} and d_{1i} are the the pulse width modulation (PWM) signals of the converter of the transformed common-mode and differential-mode at node i, respectively; and d_{pi} and d_{ni} are the PWM signals of the converter of the positive and negative poles of DG at node i, respectively.

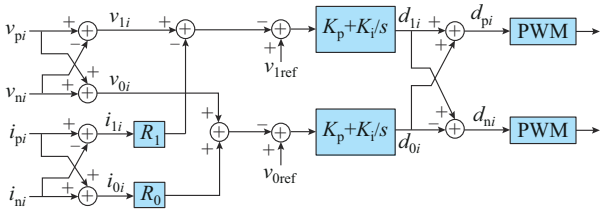

Fig. 10. Combination of traditional voltage control and modulus voltage control.

Figure 10 depicts the combination of traditional voltage control and modulus voltage control. Typically, the rated bus voltage can be chosen as the reference voltage of v_{1i}, whereas the reference voltage of v_{0i} is set to be 0. The modulus voltage control ensures that v_{pi} and v_{ni} are equal when they exceed the rated bus voltage. As a result, the unbalanced power supply can be reduced, consequently lowering the neutral current and unbalanced voltage in the load.

B. Modulus Voltage Consensus Control Approach

The consensus algorithm is adopted to develop a distributed control system for common-mode and differential-mode voltages depending on the modulus voltage control. The fundamental concept in the control system is to use the consensus algorithm to ensure that the average values are constant by collecting the modulus voltages of each node as state variables.

The bipolar DCMG with the integration of DC-ZCBs contains multiple parallel DC/DC converters with CLs. The hypothetical properties in the control system are given as follows.

1) The DC/DC converter can be regarded as an optimum controllable voltage source. The response speed of the Buck converter can be rapid enough to ignore its dynamic characteristics.

2) Since the output regulation controller of the load converter is sufficiently responsive, all loads connected to the converter can be considered as CL.

3) In the bipolar DCMG with the integration of DC-ZCBs, the inductance of the lines is negligible.

A distributed cooperative control strategy based on modulus voltage is proposed, and the stability precautions are performed to eliminate CL instability, in order to produce a balanced shunt and good load voltage regulation.

Since damping has an outstanding ability to alleviate the oscillation, virtual resistance is implemented to enhance the stability and the transient function of the system. The proposed strategy of the bipolar DCMG with the integration of DC-ZCBs is illustrated in Fig. 11 and the output modulus voltage values of each inverter are:

$$\begin{cases} v_{0i}=v_{0\text{ref}}+\delta i_{0i}+\delta v_{0i}-c_i i_{0i} \\ v_{1i}=v_{1\text{ref}}+\delta i_{1i}+\delta v_{1i}-c_i i_{1i} \end{cases} \tag{8}$$

where δi_{0i} and δi_{1i} are the common-mode and differential-mode correction currents at node i, respectively; δv_{0i} and δv_{1i} are the common-mode and differential-mode correction voltages at node i, respectively; and c_i is the virtual resistance at node i.

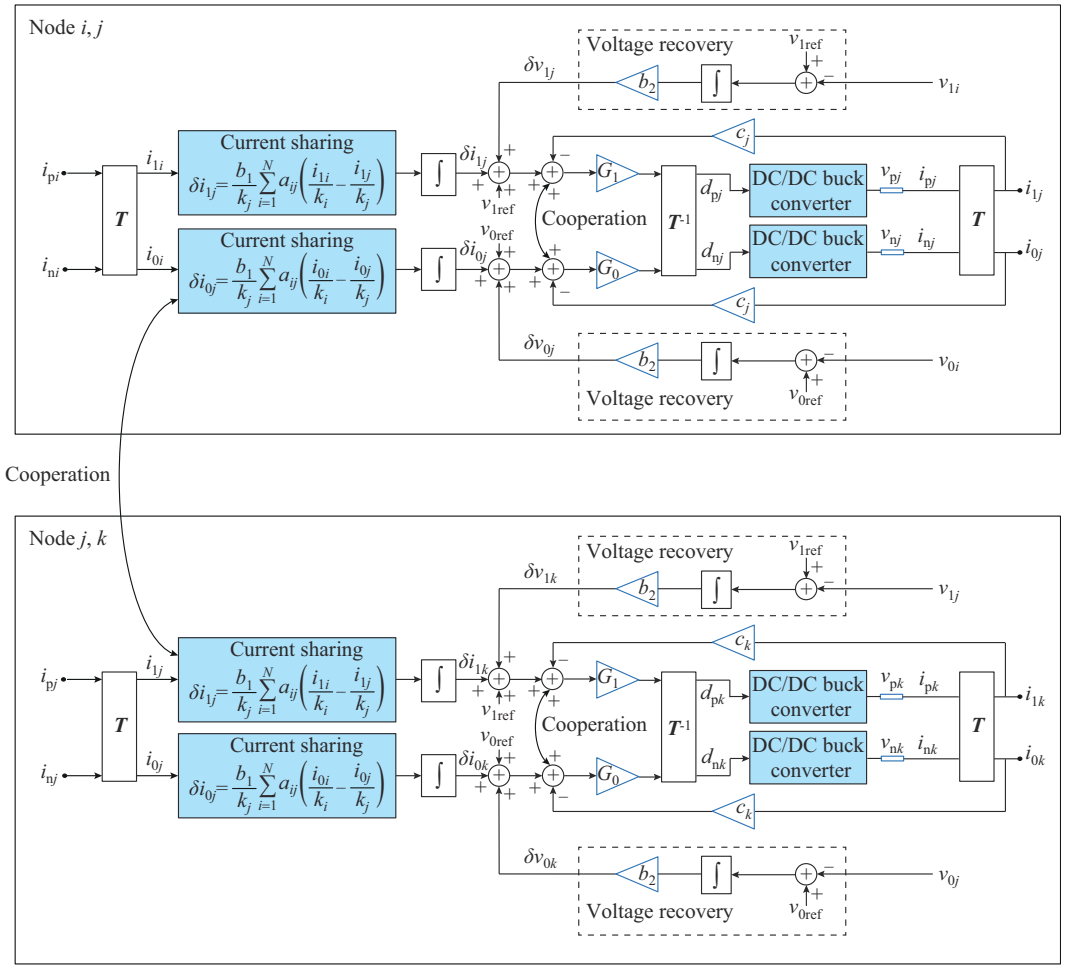

Fig. 11. Diagram of distributed cooperative control strategy.

Then, the correction currents are given as:

$$\begin{cases} \delta i_{1j} = \dfrac{b_1}{k_j}\displaystyle\sum_{i=1}^{N} a_{ij}\left(\dfrac{i_{1i}}{k_i} - \dfrac{i_{1j}}{k_j}\right) \\ \delta i_{0j} = \dfrac{b_1}{k_j}\displaystyle\sum_{i=1}^{N} a_{ij}\left(\dfrac{i_{0i}}{k_i} - \dfrac{i_{0j}}{k_j}\right) \end{cases} \tag{9}$$

where k_j is the current sharing proportional coefficient at node j; b_1 is the positive gain coefficient; and a_{ij} is the communication weight between nodes i and j, respectively.

When communication occurs between nodes i and j, $a_{ij} = a_{ji} > 0$; if no communication exists between nodes i and j, $a_{ij} = 0$. Formula (9) can be expressed in matrix form as:

$$\delta \boldsymbol{j} = -b_1 \int \boldsymbol{KLK} i \mathrm{d}t \tag{10}$$

where $\delta \boldsymbol{j} = [\delta_1, \delta_2, \ldots, \delta_N]^{\mathrm{T}}$; $\boldsymbol{K} = \mathrm{diag}\{1/k_i\}$; and $\boldsymbol{L}$ is the Laplace matrix of communication structure.

The voltage regulation is provided to derive the load correction voltage as:

$$\begin{cases} \delta v_{j1} = b_2 \displaystyle\int (v_{1\mathrm{ref}} - v_{1i})\,\mathrm{d}t \\ \delta v_{j0} = b_2 \displaystyle\int (v_{0\mathrm{ref}} - v_{0i})\,\mathrm{d}t \end{cases} \tag{11}$$

where b_2 is the additional gain factor. To increase the reliability and reduce the communication cost, two or three DGs are involved to regulate the voltage.

According to (8), (10), and (11), the common-mode and differential-mode components of the bus voltage are presented as:

$$\begin{cases} \boldsymbol{v}_1 = v_{1\mathrm{ref}} \boldsymbol{1}_N - \boldsymbol{C} i_1 + \displaystyle\int [-b_1 \boldsymbol{KLK} i_{1i} + b_2 \boldsymbol{L}(v_{1\mathrm{ref}} - v_{1i})]\mathrm{d}t \\ \boldsymbol{v}_0 = v_{0\mathrm{ref}} \boldsymbol{1}_N - \boldsymbol{C} i_0 + \displaystyle\int [-b_1 \boldsymbol{KLK} i_{0i} + b_2 \boldsymbol{L}(v_{0\mathrm{ref}} - v_{0i})]\mathrm{d}t \end{cases} \tag{12}$$

where $\boldsymbol{v}_1 = [v_{11}, v_{12}, \ldots, v_{1N}]^{\mathrm{T}}$; $\boldsymbol{v}_0 = [v_{01}, v_{02}, \ldots, v_{0N}]^{\mathrm{T}}$; $\boldsymbol{C} = \mathrm{diag}\{c_i\}$; and $\boldsymbol{1}_N$ is a column vector and each element is equal to 1. In the steady state, (12) can be expressed as:

$$\begin{cases} -b_1 \boldsymbol{KLK} i_1 + b_2 \boldsymbol{L}(v_{1\mathrm{ref}} - v_{1i}) = \boldsymbol{0}_N \\ -b_1 \boldsymbol{KLK} i_0 + b_2 \boldsymbol{L}(v_{0\mathrm{ref}} - v_{0i}) = \boldsymbol{0}_N \end{cases} \tag{13}$$

where $\boldsymbol{0}_N$ is an N-dimensional zero matrix.

According to the above analysis, the voltage and current meet:

$$\begin{cases} \dfrac{i_1}{k_1} = \dfrac{i_2}{k_2} = \ldots = \dfrac{i_N}{k_N} \\ v = v_{\mathrm{ref}} \end{cases} \tag{14}$$

The fact that not all DGs are required to participate in voltage recovery is evident from (14), which indicates that the communication cost can be reduced by using a number of nearby DGs to collect the load voltage.

IV. Consistency in Control Performance and Small-signal Stability Analysis

A. Consensus Control of DC Bus Average Voltage

The convergence of the DC bus average voltage and unbalanced voltage coefficient is demonstrated by using the Laplace transform and frequency domain analysis. The positive pole is studied first in the bipolar DCMG with the integration of DC-ZCBs, and the analysis procedure for the negative pole is the same. According to the analysis of the bipolar average unbalanced voltage in [40], the Laplace matrix of the DC bus average voltage is expressed in the frequency domain as:

$$\begin{cases} s\boldsymbol{V}_{\mathrm{ap}}-\boldsymbol{V}_{\mathrm{ap}}(0)=s\boldsymbol{V}_{\mathrm{p}}-\boldsymbol{V}_{\mathrm{p}}(0)-\boldsymbol{L}\boldsymbol{V}_{\mathrm{ap}} \\ \boldsymbol{V}_{\mathrm{ap}}=[V_{\mathrm{ap1}}, V_{\mathrm{ap2}}, \ldots, V_{\mathrm{ap}N}]^{\mathrm{T}} \\ \boldsymbol{V}_{\mathrm{p}}=[V_{\mathrm{p1}}, V_{\mathrm{p2}}, \ldots, V_{\mathrm{p}N}]^{\mathrm{T}} \end{cases} \tag{15}$$

where $\boldsymbol{V}_{\mathrm{ap}}$ and $\boldsymbol{V}_{\mathrm{p}}$ are the Laplace transforms of $v_{\mathrm{ap}N}$ and $v_{\mathrm{p}N}$, respectively.

The initial condition is satisfied with $\boldsymbol{V}_{\mathrm{ap}}(0)=\boldsymbol{V}_{\mathrm{p}}(0)$.

$$\boldsymbol{V}_{\mathrm{ap}}=s(s\boldsymbol{E}+\boldsymbol{L})^{-1}\boldsymbol{V}_{\mathrm{p}} \tag{16}$$

where $\boldsymbol{E}$ is the identity matrix.

According to the characteristics of $\boldsymbol{L}$, when $\boldsymbol{L}$ is balanced, $\boldsymbol{V}_{\mathrm{ap}}$ will converge to a value, i. e., the true average voltage $\boldsymbol{V}_{\mathrm{amp}}$.

$$\boldsymbol{V}_{\mathrm{amp}}=\lim_{t\to\infty}\boldsymbol{V}_{\mathrm{ap}}(t)=\lim_{s\to 0}s\boldsymbol{V}_{\mathrm{ap}}=\lim_{s\to 0}s(s\boldsymbol{E}+\boldsymbol{L})^{-1}\cdot\lim_{s\to 0}s\boldsymbol{V}_{\mathrm{p}}=\boldsymbol{Q}\boldsymbol{v}_{\mathrm{mp}}=\left\langle \boldsymbol{v}_{\mathrm{mp}}\right\rangle\boldsymbol{1}_N \tag{17}$$

where $\boldsymbol{v}_{\mathrm{amp}}=[v_{\mathrm{amp1}}, v_{\mathrm{amp2}}, \ldots v_{\mathrm{amp}N}]^{\mathrm{T}}$; and $\boldsymbol{Q}$ is the mean matrix and all the elements are $1/N$. The steady-state value of vector $\boldsymbol{v}_{\mathrm{ap}}$ is denoted as $\boldsymbol{v}_{\mathrm{amp}}$. The mean of each element of vector $\boldsymbol{v}_{\mathrm{mp}}$ is represented by $\left\langle \boldsymbol{v}_{\mathrm{mp}}\right\rangle$:

$$\left\langle \boldsymbol{v}_{\mathrm{mp}}\right\rangle=\frac{1}{N}\sum_{i=1}^{N}v_{\mathrm{mp}i} \tag{18}$$

B. Consensus Control of Unbalanced Voltage Coefficient

Based on the analysis of the control approach presented in [40], the differential-positive voltage and differential-negative voltage are expressed by the Laplace matrix, and then the equivalent arrangement in the frequency domain can be obtained as:

$$\boldsymbol{V}_{\mathrm{un}}=s(s\boldsymbol{E}-\boldsymbol{L})^{-1}\boldsymbol{V}'_{\mathrm{un}}=\boldsymbol{H}_{\mathrm{un}}\boldsymbol{V}'_{\mathrm{un}} \tag{19}$$

where $\boldsymbol{V}_{\mathrm{un}}$ and $\boldsymbol{V}'_{\mathrm{un}}$ are the Laplace transforms of $\boldsymbol{v}_{\mathrm{un}}$ and $\boldsymbol{v}'_{\mathrm{un}}$, respectively, $\boldsymbol{v}_{\mathrm{un}}=[v_{\mathrm{un1}}, v_{\mathrm{un2},} \ldots, v_{\mathrm{un}N}]^{\mathrm{T}}$, and $\boldsymbol{v}'_{\mathrm{un}}=[v'_{\mathrm{un1}}, v'_{\mathrm{un2}}, \ldots, v'_{\mathrm{un}N}]^{\mathrm{T}}$.

When DCMG is balanced, $\boldsymbol{v}_{\mathrm{un}}$ will converge to the value $\boldsymbol{v}_{\mathrm{mun}}$.

$$\boldsymbol{v}_{\mathrm{mun}}=\lim_{t\to\infty}\boldsymbol{v}_{\mathrm{un}}(t)=\lim_{s\to 0}s\boldsymbol{V}_{\mathrm{un}}=\lim_{s\to 0}s(s\boldsymbol{E}-\boldsymbol{L})^{-1}\cdot\lim_{s\to 0}s\boldsymbol{V}'_{\mathrm{un}}=\boldsymbol{Q}\boldsymbol{v}'_{\mathrm{un}}=\left\langle \boldsymbol{v}'_{\mathrm{mum}}\right\rangle\boldsymbol{1}_n \tag{20}$$

where $\boldsymbol{v}_{\mathrm{mun}}=[v_{\mathrm{mun1}}, v_{\mathrm{mun2}}, \ldots, v_{\mathrm{mun}N}]^{\mathrm{T}}$; and $\boldsymbol{v}'_{\mathrm{mun}}$ is the Laplace transforms of $\boldsymbol{v}_{\mathrm{mun}}$, $\boldsymbol{v}'_{\mathrm{mun}}=[v'_{\mathrm{mum1}}, v'_{\mathrm{mum2}}, \ldots, v'_{\mathrm{mum}N}]^{\mathrm{T}}$.

C. Analysis of Steady-state Operation Point

Consensus analysis is applied to examine the steady-state operation point in the bipolar DCMG while taking into account the consensus algorithm. According to the proposed strategy, the positive correction voltage in [40] can be expressed as:

$$\begin{cases} \boldsymbol{\delta}'_{\mathrm{p}}=\boldsymbol{G}_{\mathrm{u}}(\boldsymbol{V}_{\mathrm{refp}}-\boldsymbol{V}_{\mathrm{ap}}) \\ \boldsymbol{\delta}''_{\mathrm{p}}=\boldsymbol{G}_{\mathrm{o}}(f_1(\boldsymbol{V}'_{\mathrm{un}})\boldsymbol{V}_{\mathrm{n}}-\boldsymbol{V}_{\mathrm{p}}) \end{cases} \tag{21}$$

where $\boldsymbol{V}_{\mathrm{refp}}=(v_{\mathrm{refp}}/s)\boldsymbol{1}_N$ is the reference value of positive bus voltage; and $\boldsymbol{G}_{\mathrm{o}}=\mathrm{diag}\{G_{oi}\}$ and $\boldsymbol{G}_{\mathrm{u}}=\mathrm{diag}\{G_{ui}\}$ are the transfer function matrices for DC bus average voltage controller and unbalanced controller, respectively.

$$\begin{cases} G_{ui}=k_{\mathrm{pVp}i}+\dfrac{k_{\mathrm{iVp}i}}{s} \\ G_{oi}=k_{\mathrm{punp}i}+\dfrac{k_{\mathrm{iunp}i}}{s} \end{cases} \tag{22}$$

Considering the system voltage droop control at the same time, the positive reference voltage $\boldsymbol{V}_{\mathrm{p}}^{*}$ for voltage droop control of the bipolar DCMG meets:

$$\boldsymbol{V}_{\mathrm{p}}^{*}=\boldsymbol{V}_{\mathrm{refp}}+\boldsymbol{\delta}'_{\mathrm{p}}+\boldsymbol{\delta}''_{\mathrm{p}}-\boldsymbol{R}_{\mathrm{dp}}\boldsymbol{I}_{\mathrm{loadp}} \tag{23}$$

where $\boldsymbol{R}_{\mathrm{dp}}=\mathrm{diag}\{R_{\mathrm{dp}}\}$ is the droop gain matrix; $\boldsymbol{I}_{\mathrm{loadp}}$ is Laplace transform of positive load current $\boldsymbol{i}_{\mathrm{loadp}}$, $\boldsymbol{i}_{\mathrm{loadp}}=[i_{\mathrm{loadp1}}, i_{\mathrm{loadp2}}, \ldots, i_{\mathrm{loadp}N}]^{\mathrm{T}}$.

The steady-state characteristics of positive average voltage is obtained in (24), with the derivation process detailed in Supplementary Material A.

$$\boldsymbol{V}_{\mathrm{amp}}=\left\langle V_{\mathrm{amp}}\right\rangle\boldsymbol{1}_N=V_{\mathrm{refp}}\boldsymbol{1}_N \tag{24}$$

Similarly, the steady-state characteristics of negative voltage can be obtained as:

$$\boldsymbol{V}_{\mathrm{amn}}=\left\langle V_{\mathrm{amn}}\right\rangle\boldsymbol{1}_N=V_{\mathrm{refn}}\boldsymbol{1}_N \tag{25}$$

It is proven by the derivation that the average node voltages $v_{\mathrm{ap}i}$ and $v_{\mathrm{an}i}$ tend to be converged and remain uniform under the steady state in bipolar DCMG. Specifically, $v_{\mathrm{ap}i}$ and $v_{\mathrm{an}i}$ will be stabilized at the positive and negative rated reference voltages V_{refp} and V_{refn}, respectively. The correctness of the proposed strategy is thus confirmed.

D. Analysis of Small-signal Stability

To investigate the small-signal stability in bipolar DCMGs, this paper establishes a small-signal model and analyzes the impact of the system stability under the proposed strategy through Nyquist analysis. The derivation process of the output characteristics and the transfer function from the control to the output of DC/DC converters is provided in Supplementary Material A.

The structure diagram of the primary control can be obtained, as shown in Fig. 12(a). The input of the system is the reference voltage $\hat{v}_{0\mathrm{ref}}^{*}(s)$ (or $\hat{v}_{1\mathrm{ref}}^{*}(s)$), and the output is the node voltage $\hat{v}_0(s)$ (or $\hat{v}_1(s)$). Simplifying the block diagram, taking $\hat{v}_{0\mathrm{ref}}^{*}(s)$ (or $\hat{v}_{1\mathrm{ref}}^{*}(s)$) as input and $\hat{v}_0(s)$ (or $\hat{v}_1(s)$) as output, the transfer functions of primary control are derived as:

$$\begin{cases} G_0 = \dfrac{2k_pV_sR(3R+R_L)s+2k_iV_sR(3R+R_L)}{CLR(3R+R_L)s^3+LRs^2+(3R^2+RR_L+6k_pV_sr_dR+2k_pr_dR_LV_s)s+2k_ir_dV_s(3R+R_L)} \\ G_1 = \dfrac{2k_pV_sR(R+R_L)s+2k_iV_sR(R+R_L)}{CLR(R+R_L)s^3+LRs^2+(R^2+RR_L+2k_pV_sr_dR+2k_pr_dR_LV_s)s+2k_ir_dV_s(R+R_L)} \end{cases} \tag{26}$$

where G_0 and G_1 are the common-mode and differential-mode transfer functions of the primary control, respectively. Combining and simplifying (S11), (S12) in Supplementary Material A, and (26) with (9)-(11), the block diagram of the bipolar DCMG with secondary control is obtained, as shown in Fig. 12(b). The common-mode control black diagram is taken as an example in Fig. 12, and the differential-mode control block diagram is similar. By combining (9) between the average DC bus voltage and the DC bus voltage, we can simplify the system transfer function with common-mode reference voltage $\hat{v}_{0\mathrm{ref}}(s)$ as input and common-mode average voltage $\hat{v}_{\mathrm{ave0}}(s)$ and common-mode average current $\hat{i}_{\mathrm{ave0}}(s)$ as outputs. The system is then subjected to small-signal stability analysis.

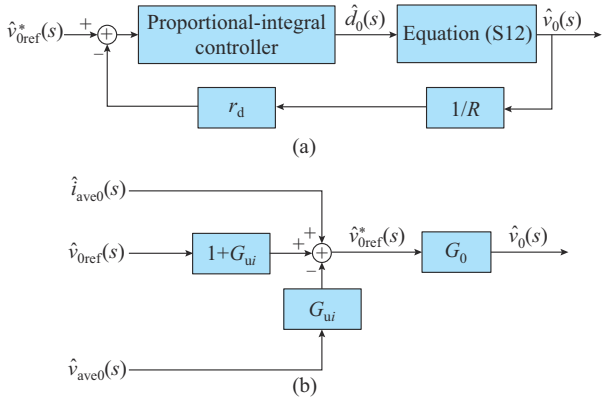

Fig. 12. Block diagram of control system including proposed strategy. (a) Primary control approach (positive pole). (b) With integration of secondary control approach.

Due to the modulus voltage consensus control, the control systems of the DC/DC converters interconnected through the communication system are mutually coupled. This paper verifies the stability of the proposed strategy for a bipolar DCMG with three converters connected to each other through a communication system. The three nodes are indexed by x, y, and z.

From Fig. 12(b), it can be observed that due to the modulus voltage consensus control, the control-to-output transfer function of the bipolar DCMG including the primary control and secondary control needs to take into account the communication of the three nodes. In this paper, we take node x as an example to analyze the stability of node x by considering the control influence of nodes y and z on node x, and then extend it to the stability of the entire system. The impacts of the modulus voltage consensus control of nodes y and z on node x are defined as $C_{x,y}$ and $C_{x,z}$, respectively.

To study the influence of the modulus voltage consensus control coefficients a_{ij} on the stability of bipolar DCMG, the values of a_{ij} are set to be the same, and Nyquist curves for various interaction terms are plotted under different a_{ij}, as shown in Fig. 13. Due to symmetry, the results of $C_{x,y}$ and $C_{x,z}$ are the same, so only $C_{x,y}$ is given. As can be observed from Fig. 13, as a_{ij} increases, $C_{x,x}$ and $C_{x,y}$ gradually increase but do not encircle the (−1, j0) point, and the system is stable.

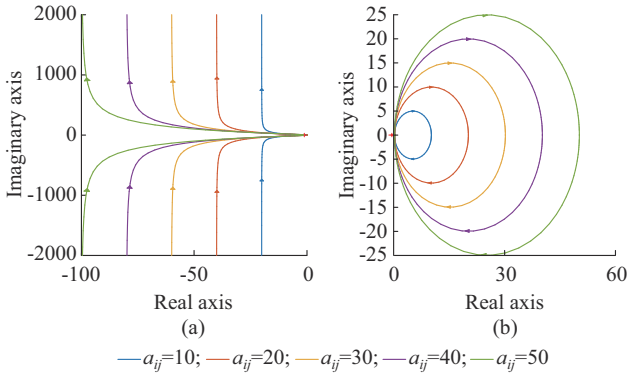

Fig. 13. Nyquist curves under different a_{ij}. (a) $C_{x,x}$. (b) $C_{x,y}$.

The following analysis focuses on the control-to-output analysis of the bipolar DCMG considering the modeling of converters, primary control, and secondary control. Based on Fig. 13(b), the control-to-output transfer function of the common-mode control loop of node x can be written as:

$$\hat{v}_{x0} = f_{x,x}(\hat{v}_{x0\mathrm{ref}}) + f_{x,y}(\hat{v}_{y0\mathrm{ref}}) + f_{x,z}(\hat{v}_{z0\mathrm{ref}}) \tag{27}$$

It can be observed from (27) that nodes y and z generate interaction terms for node x. To verify the impact of control parameters on stability, the effect of voltage recovery control is examined. Different coefficients b of the voltage recovery control are set, and Nyquist curves for the control-to-output of the nodes are shown in Fig. 14. From Fig. 14, as b increases, the Nyquist curve gradually begins to encircle the (−1, j0) point. When $b=1$, the Nyquist curve passes through the (−1, j0) point. When $b=2$, the Nyquist curve encircles the (−1, j0) point. Therefore, to ensure the stability of bipolar DCMG, the value of b should be set less than 1.

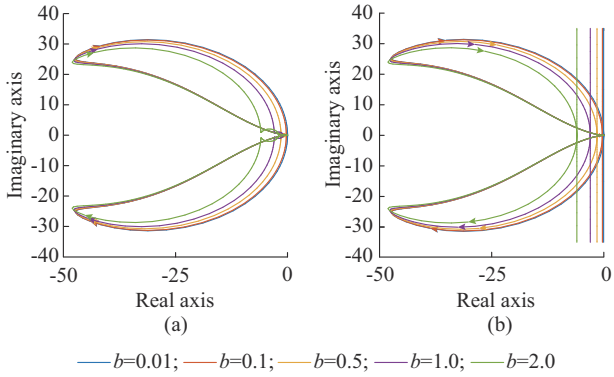

Fig. 14. Nyquist curves under different b. (a) $f_{x,x}$. (b) $f_{x,y}$.

V. Simulation Results

A topology of the bipolar DCMG with the integration of DC-ZCBs is designed by using MATLAB/Simulink to verify the efficacy of the proposed strategy, as depicted in Fig. 15. The loads at the positive node are $R_{p1}=5\ \Omega$, $R_{p2}=10\ \Omega$, $R_{p3}=20\ \Omega$, and $R_{p4}=20\ \Omega$, while the loads at the negative node are $R_{n1}=10\ \Omega$, $R_{n2}=20\ \Omega$, $R_{n3}=20\ \Omega$, and $R_{n4}=10\ \Omega$. The relevant system parameters and control parameters are provided in Table II.

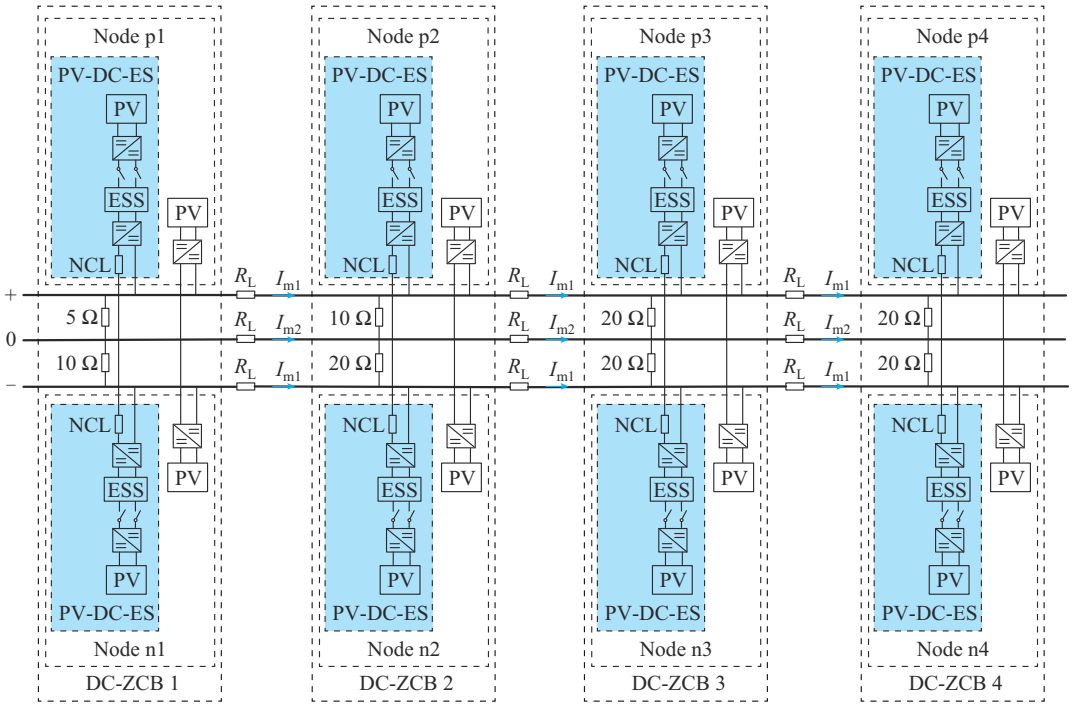

Fig. 15. Topology of bipolar DCMG with integration of DC-ZCBs.

TABLE II
System Parameters and Control Parameters

Parameters	Value	Parameters	Value
V_{ref}	400 V	R_L	0.1 Ω
R_{NCL}	20 Ω	r_d	0.05 Ω
k_p	0.1	k_i	0.01
a_{ij}	10	b	0.5
C_f	200 μF	L_f	50 mH

A. Validation of Effectiveness of Proposed Strategy

Figure 16 presents the simulation results obtained from traditional voltage droop control, which is added to the control system after 3 s.

In Fig. 16(a) and (b), v_p and v_n are less than 400 V. An increase in voltage drop between the DG side and the load side can result in an increase in voltage deviation. In contrast, Fig. 16(c) shows that the traditional voltage droop control effectively suppresses the overall unbalanced voltage coefficient ε_u across 4 nodes. In Fig. 16(d), the neutral line currents I_{m1}-I_{m3} vary with the unbalanced voltage coefficient depicted in Fig. 16(c). Although traditional voltage droop control can suppress the unbalanced voltage coefficient to some extent, v_p and v_n still remain below the rated voltage of 400 V.

Figure 17 depicts the comparison of simulation results between traditional voltage droop control and proposed strategy, where only traditional voltage droop control is applied from 1 s to 3 s, and the proposed strategy is used from 3 s. According to the results, the proposed strategy effectively compensates for the voltage at the load side. Figure 17(a) and (b) shows that v_p and v_n are both increased under the proposed strategy, indicating improved voltage compensation at the load side. In addition, Fig. 17(c) and (d) demonstrates that the average common-mode voltage v_{av0} is maintained at 0 V, while the average differential-mode voltage v_{av1} of nodes 1-4 increases from 398 V to 400 V under the proposed strategy. These findings illustrate that the proposed strategy is capable of correcting the voltage at the load side, making it an effective strategy for the bipolar DCMG with the integration of DC-ZCBs.

B. Performance Comparisons with Other Advanced Voltage Control Approaches

1) Comparison with Consensus-based Distributed Control Approach [32]

In [32], a consensus-based distributed control approach for DGs in bipolar DCMG is presented to mitigate the unbalanced voltage. To highlight the superiority of the proposed strategy in this paper, a comparison is conducted in this part with the approach in [32]. The simulation model remains the same, as shown in Table II. The system utilizes the consensus-based distributed control approach in [32] during the initial 3 s and transitions to the proposed modulus voltage consensus control approach thereafter. The comparative results between consensus-based distributed control approach in [32] and proposed modulus voltage consensus control approach are depicted in Fig. 18.

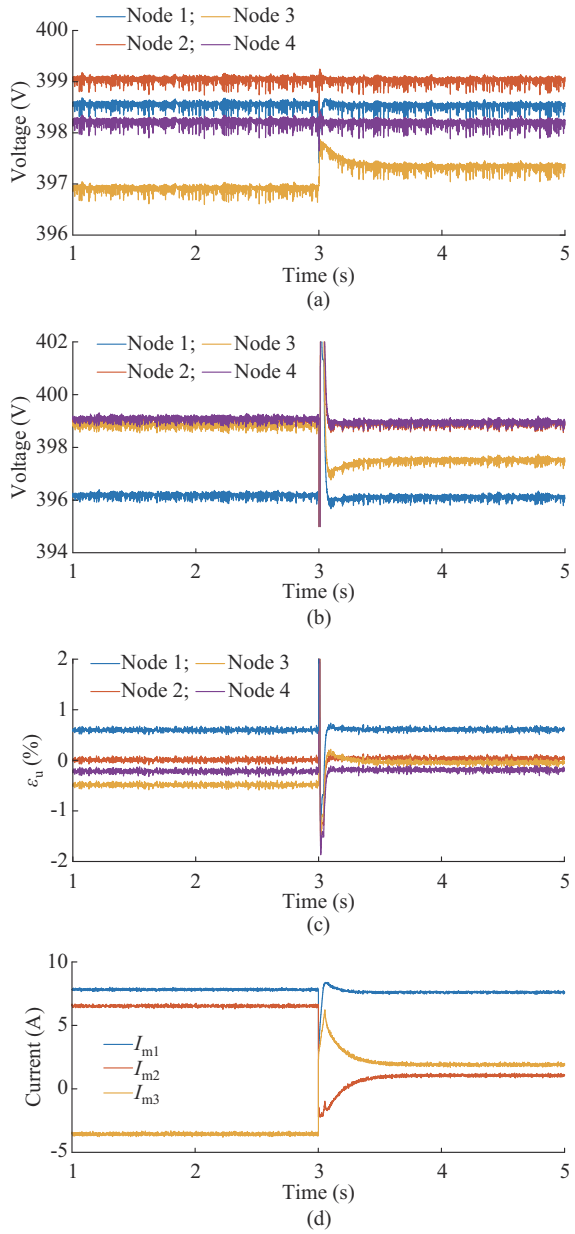

Fig. 16. Simulation results obtained from traditional voltage droop control. (a) v_p. (b) v_n. (c) ε_u. (d) I_m.

In Fig. 18(a) and (b), v_p and v_n under the consensus-based distributed control approach in [32] deviate further from the rated voltage than those under the proposed modulus voltage consensus control approach. Figure 18(c) and (d) shows that the modulus voltage consensus control approach can ensure that the average positive voltage v_{avp} and average negative voltage v_{avn} of different nodes are consistent. Thus, the proposed modulus voltage consensus control approach can reduce the impact of the unbalanced components between DGs, resulting in a reasonably independent control of the positive and negative DGs as well as a weakening of the coupling between the controls.

Figure 19 presents ε_u under conditions *a* and *b*, which are specifically before 3 s and after 3 s. The results demonstrate that ε_u of each node is significantly smaller when the proposed modulus voltage consensus control approach is applied. Hence, the proposed modulus voltage consensus control approach is highly effective in reducing ε_u.

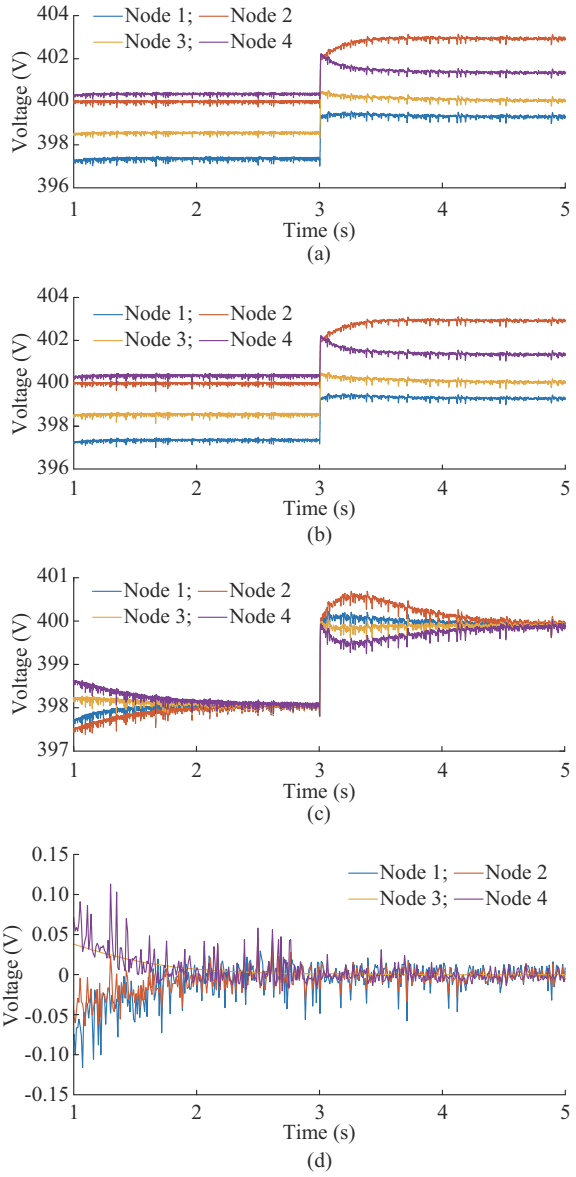

Fig. 17. Comparison of simulation results between traditional voltage droop control and proposed strategy. (a) v_p. (b) v_n. (c) v_{av1}. (d) v_{av0}.

In a bipolar DCMG with the integration of DC-ZCBs, the magnitude of the neutral current I_m has an impact on the losses of the bipolar DCMG. When the output voltages of the DGs in the bipolar DCMG with the integration of DC-ZCBs are equalized, I_m will be further reduced. The comparison of neutral line current when load changes under conditions *a* and *b* are shown in Fig. 20. According to Fig. 20, under condition *a*, I_m is not equal to 0 and can even reach a maximum current of 9.5 A. In contrast, I_m is always very small under condition *b*. The proposed strategy can further regulate the neutral current, thereby reducing the operational losses of the bipolar DCMG.

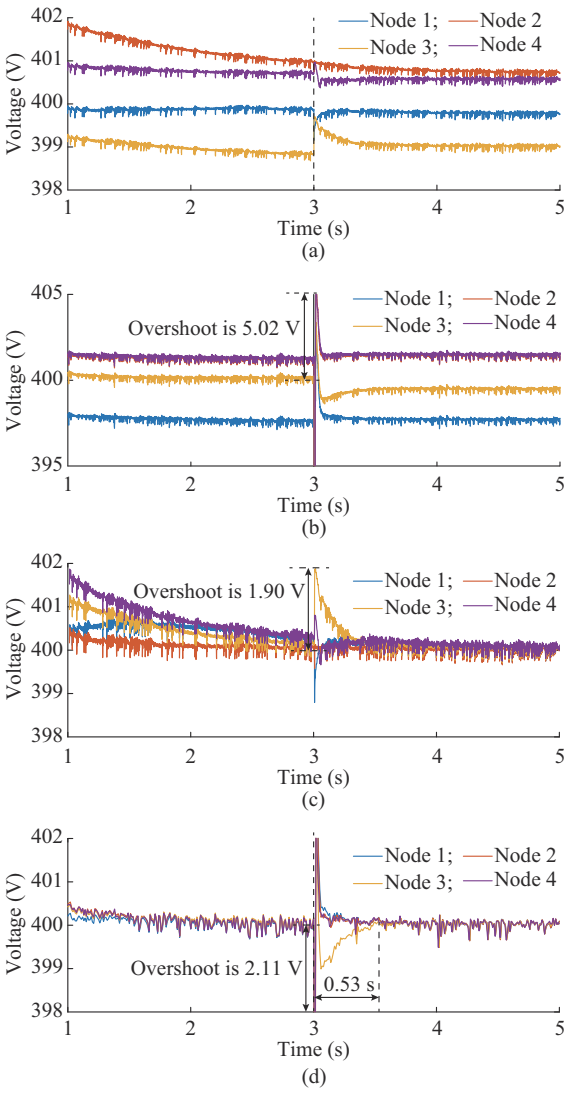

Fig. 18. Comparative results between consensus-based distributed control in [32] and proposed modulus control. (a) v_p. (b) v_n. (c) v_{avp}. (d) v_{avn}.

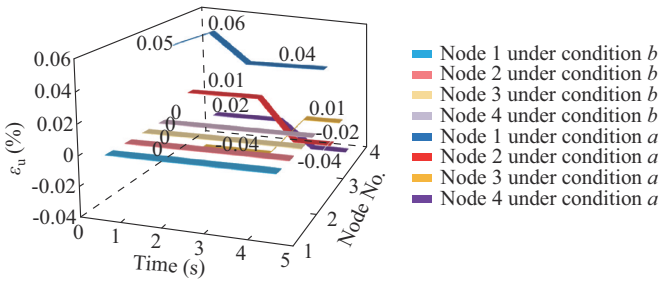

Fig. 19. Unbalanced voltage coefficient under conditions *a* and *b*.

2) Comparison with Adaptive Droop Control Approach of Unbalanced Voltage Based on Fuzzy Control

In this part, a comparison is made with the adaptive droop control of unbalanced voltage based on fuzzy control proposed in [24]. The line resistance is set as 0.1 Ω, and other parameters of the model are the same as those in Table II. The calculated unbalanced voltage coefficients are presented in Fig. 21, where ε_{u1} and ε_{u2} represent the simulated results of the unbalanced voltage coefficients obtained by adaptive droop control of unbalanced voltage based on fuzzy control and the proposed strategy, respectively. From Fig. 21, it can be observed that the proposed strategy effectively suppresses the unbalanced voltage coefficients at various nodes. Specifically, the unbalanced voltage coefficients at node 3 are significantly suppressed. Although there is a slight increase in the unbalanced voltage coefficients at node 2, it remain at very low magnitudes. After using the proposed strategy, the average unbalanced voltage coefficient of the nodes is reduced from 0.62% to 0.41%, a decrease of 34%.

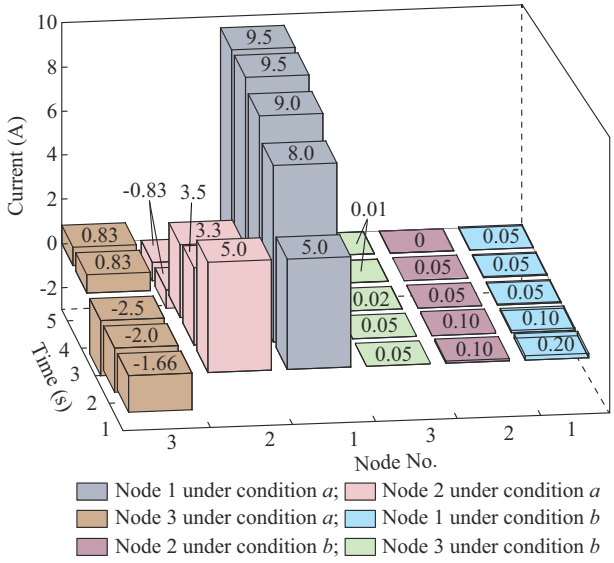

Fig. 20. Comparison of neutral line current when load changes under conditions *a* and *b*.

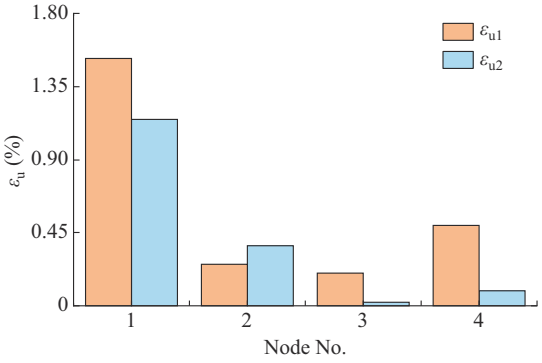

Fig. 21. Comparison of results between adaptive droop control approach and proposed strategy.

C. Impact of Load Variations on Bipolar DCMG with Integration of DC-ZCBs Under Proposed Strategy

In Sections V-A and V-B, the proposed strategy is shown to be superior to both positive and negative voltage control approaches as well as other advanced voltage control approaches. This subsection focuses on investigating its effectiveness under load variations on the bipolar DCMG with integration of DC-ZCBs. At 3 s, a 10 Ω resistance is added at the positive terminal at node 4. Figure 22 shows the effect of load variation under proposed strategy. In Fig. 22(a) and (b), it is evident that v_p and v_n at all nodes stay constant after load variation at 3 s. Figure 22(c) and (d) demonstrates

that v_{av1} remains at the rated voltage of 400 V, and v_{av0} remains at 0 V, which is consistent with the control objectives.

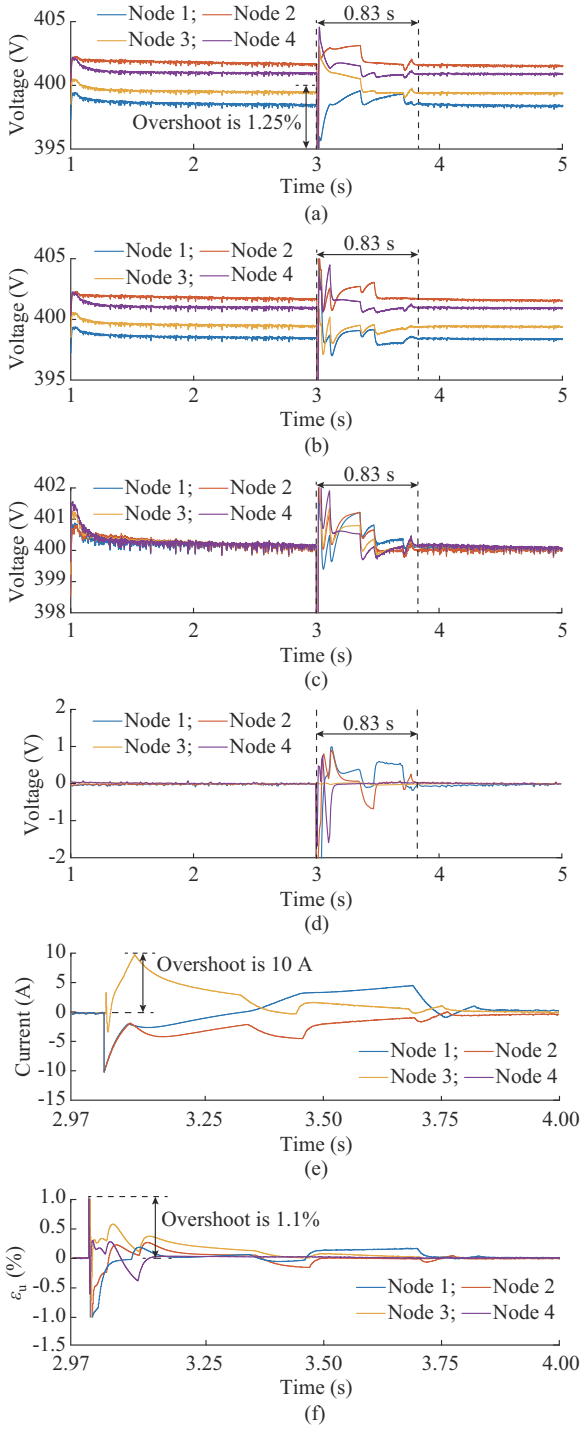

Fig. 22. Effect of load variation under proposed strategy. (a) v_p. (b) v_n. (c) v_{av1}. (d) v_{av0}. (e) i_m. (f) ε_u.

Based on the proposed strategy, Fig. 23 presents the effect of load variation on ε_u of bipolar DCMG with the integration of DC-ZCBs under proposed strategy. All the ε_u of nodes 1-4 is kept at 0 before switching the load under the proposed strategy. After the additional load is added at 3 s, ε_u increases slightly, but remains well below the rated value of 3. Subsequently, all the ε_u of nodes 1-4 is back to 0 at 5 s.

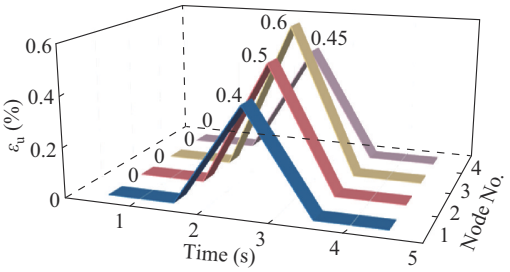

Fig. 23. Effect of load variation on ε_u of bipolar DCMG with integration of DC-ZCBs under proposed strategy.

The values of I_m for the bipolar DCMG with integration of DC-ZCBs are presented in Fig. 24. Similar to the results in Fig. 23, the neutral line currents only increase at 3 s when the additional load is switched. Therefore, it verifies the validity of the proposed strategy even under load variations.

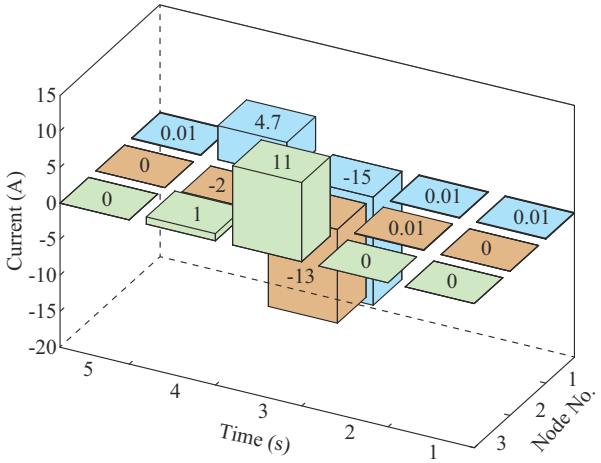

Fig. 24. Effect of load variation on neutral line current of bipolar DCMG with integration of DC-ZCBs under proposed strategy.

VI. Conclusion

With the acceleration of energy transition, ZCBs and localized bipolar DCMGs develop rapidly. However, this growth introduces challenges to unbalanced voltage suppression caused by high penetration of RESs. Considering this scenario, this paper proposes a distributed cooperative control strategy for DC-ESs based on the modulus voltage in bipolar DCMGs with the integration of ZCBs. The topological structure of the PV-DC-ES is introduced, which improves the absorption capacity of renewable energy and reduces the capacity and volume of the ESS of DC-ES. A mathematical equivalent model for a bipolar DCMGs incorporating PV-DC-ES is established. The coupling characteristics and influencing factors within the bipolar DCMGs system are discussed. Based on this, the proposed strategy of PV-DC-ES effectively decouples the control system of the bipolar DCMG, simplify the control architecture and efficiently suppress unbalanced voltage. Through a comparative analysis with a state-of-art control approaches, the results of this paper demonstrate that the proposed strategy significantly suppresses unbalanced voltage of the system. Furthermore, unbalanced cur-

rent and power losses are also significantly reduced.

REFERENCES

[1] R. Wang, W. Feng, H. Xue *et al*., "Simulation and power quality analysis of a loose-coupled bipolar DC microgrid in an office building," *Applied Energy*, vol. 303, p. 117606, Dec. 2021.

[2] R. Brown, V. Vossos, J. Kloss *et al*. (2017, May). Review of DC power distribution in buildings: a technology and market assessment. [Online]. Available: https://eta.lbl.gov/publications?author=Vagelis%20Vossos

[3] H. J. Byun, J. M. Park, B. J. Kim *et al*., "Small signal modeling of interleaved voltage balancer with coupled-inductor," in *Proceedings of 2020 IEEE Electric Power and Energy Conference*, Edmonton, Canada, Nov. 2020, pp. 1-6.

[4] J. Yang, X. Jin, X. Wu *et al*., "Decentralised control method for DC microgrids with improved current sharing accuracy," *IET Generation, Transmission & Distribution*, vol. 11, no. 3, pp. 696-706, Feb. 2017.

[5] X. Li, L. Guo, S. Zhang *et al*., "Observer-based DC voltage droop and current feed-forward control of a DC microgrid," *IEEE Transactions on Smart Grid*, vol. 9, no. 5, pp. 5207-5216, Sept. 2018.

[6] R. K. Chauhan, K. Chauhan, B. R. Subrahmanyam *et al*., "Distributed and centralized autonomous DC microgrid for residential buildings: a case study," *Journal of Building Engineering*, vol. 27, p. 100978, Jan. 2020.

[7] D. L. Gerber, O. A. Ghatpande, M. Nazir *et al*., "Energy and power quality measurement for electrical distribution in AC and DC microgrid buildings," *Applied Energy*, vol. 308, p. 118308, Feb. 2022.

[8] R. Galvin, "Net-zero-energy buildings or zero-carbon energy systems? How best to decarbonize Germany's thermally inefficient 1950s-1970s-era apartments," *Journal of Building Engineering*, vol. 54, p. 104671, Aug. 2022.

[9] X. Li, K. L. Wong, T. C. Y. Lau *et al*., "An ultra-efficient and low-cost solid-state circuit breaker for LVDC microgrid applications," in *Proceedings of 2021 IEEE Fourth International Conference on DC Microgrids*, Arlington, USA, Jul. 2021, pp. 1-6.

[10] M. Xu, K. Ma, B. Liu *et al*., "Modeling and correlation of two thermal paths in frequency-domain thermal impedance model of power module," *IEEE Journal of Emerging and Selected Topics in Power Electronics*, vol. 9, no. 4, pp. 3971-3981, Aug. 2021.

[11] J. Ma, M. Zhu, Q. Li *et al*., "From 'voltage balancer' to 'interlinking converter' – a shift of operation concept for distributed bipolar DC system," in *Proceedings of 43rd Annual Conference of the IEEE Industrial Electronics Society*, Beijing, China, Oct. 2017, pp. 1166-1171.

[12] S. Rivera, B. Wu, S. Kouro *et al*., "Electric vehicle charging station using a neutral point clamped converter with bipolar DC bus," *IEEE Transactions on Industrial Electronics*, vol. 62, no. 4, pp. 1999-2009, Apr. 2015.

[13] Y. Gu, W. Li, and X. He, "Analysis and control of bipolar LVDC grid with DC symmetrical component method," *IEEE Transactions on Power Systems*, vol. 31, no. 1, pp. 685-694, Jan. 2016.

[14] S. Cui, J. H. Lee, J. Hu *et al*., "A modular multilevel converter with a zigzag transformer for bipolar MVDC distribution systems," *IEEE Transactions on Power Electronics*, vol. 34, no. 2, pp. 1038-1043, Feb. 2019.

[15] Z. Zhang, D. Shi, C. Jin *et al*., "Droop control of a bipolar dc microgrid for load sharing and voltage balancing," in *Proceedings of 2017 IEEE 3rd International Future Energy Electronics Conference and ECCE Asia*, Kaohsiung, China, Jun. 2017, pp. 795-799.

[16] X. Yang, Y. Xue, B. Chen *et al*., "An enhanced reverse blocking MMC with DC fault handling capability for HVDC applications," *Electric Power Systems Research*, vol. 163, pp. 706-714, Oct. 2018.

[17] S. Kim, H. Cha, and H. G. Kim, "High-efficiency voltage balancer having DC-DC converter function for EV charging station," *IEEE Journal of Emerging and Selected Topics in Power Electronics*, vol. 9, no. 1, pp. 812-821, Feb. 2021.

[18] T. H. Jung, G. H. Gwon, C. H. Kim *et al*., "Voltage regulation method for voltage drop compensation and unbalance reduction in bipolar low-voltage DC distribution system," *IEEE Transactions on Power Delivery*, vol. 33, no. 1, pp. 141-149, Feb. 2018.

[19] S. D. Tavakoli, M. Mahdavyfakhr, M. Hamzeh *et al*., "A unified control strategy for power sharing and voltage balancing in bipolar DC microgrids," *Sustainable Energy, Grids and Networks*, vol. 11, pp. 58-68, Sept. 2017.

[20] G. H. Gwon, C. H. Kim, Y. S. Oh *et al*., "Mitigation of voltage unbalance by using static load transfer switch in bipolar low voltage DC distribution system," *International Journal of Electrical Power and Energy Systems*, vol. 90, pp. 158-167, Sept. 2017.

[21] Z. Li, S. Hoshina, N. Satake *et al*., "DC/DC converter development for battery energy storage supporting railway DC feeder system," in *Proceedings of 2015 9th International Conference on Power Electronics and ECCE Asia*, Seoul, South Korea, Jun. 2015, pp. 1655-1660.

[22] C. Guo, Y. Wang, and J. Liao, "Coordinated control of voltage balancers for the regulation of unbalanced voltage in a multi-node bipolar DC distribution network," *Electronics*, vol. 11, no. 1, p. 166, Jan. 2022.

[23] J. Liao, N. Zhou, Y. Huang *et al*., "Decoupling control for DC electric spring-based unbalanced voltage suppression in a bipolar DC distribution system," *IEEE Transactions on Industrial Electronics*, vol. 68, no. 4, pp. 3239-3250, Apr. 2021.

[24] C. Guo, J. Liao, and Y. Zhang, "Adaptive droop control of unbalanced voltage in the multi-node bipolar DC microgrid based on fuzzy control," *International Journal of Electrical Power & Energy Systems*, vol. 142, p. 108300, Nov. 2022.

[25] S. Augustine, M. K. Mishra, and N. Lakshminarasamma, "Adaptive droop control strategy for load sharing and circulating current minimization in low-voltage standalone DC microgrid," *IEEE Transactions on Sustainable Energy*, vol. 6, no. 1, pp. 132-141, Jan. 2015.

[26] H. Kakigano, Y. Miura, and T. Ise, "Distribution voltage control for DC microgrids using fuzzy control and gain-scheduling technique," *IEEE Transactions on Power Electronics*, vol. 28, no. 5, pp. 2246-2258, May 2013.

[27] W. Hatahet, M. I. Marei, and M. Mokhtar, "Adaptive controllers for grid-connected DC microgrids," *International Journal of Electrical Power & Energy Systems*, vol. 130, p. 106917, Sept. 2021.

[28] M. Mokhtar, M. I. Marei, and A. A. El-Sattar, "Improved current sharing techniques for DC microgrids," *Electric Power Components and Systems*, vol. 46, no. 7, pp. 757-767, Apr. 2018.

[29] S. Umayal, P. Selvakumar, and V. Ramkumar, "Multiple input Fuzzy controlled DC-DC Converter for harvesting renewable energy," in *Proceedings of 2021 7th International Conference on Electrical Energy Systems*, Chennai, India, Feb. 2021, pp. 329-333.

[30] J. Liao, N. Zhou, and Q. Wang, "DC grid protection method based on phase planes of single-end common-and differential-mode components," *IEEE Transactions on Power Delivery*, vol. 36, no. 1, pp. 299-310, Feb. 2021.

[31] J. Liao, C. Guo, N. Zhou *et al*., "Enhanced voltage control of bipolar DC distribution system based on modulus decomposition," *IEEE Journal of Emerging and Selected Topics in Industrial Electronics*, vol. 3, no. 4, pp. 1137-1148, Oct. 2022.

[32] X. Chen, M. Shi, J. Zhou *et al*., "Consensus-based distributed control for photovoltaic-battery units in a DC microgrid," *IEEE Transactions on Industrial Electronics*, vol. 66, no. 10, pp. 7778-7787, Oct. 2019.

[33] A. Hosseinipour and H. Hojabri, "Small-signal stability analysis and active damping control of DC microgrids integrated with distributed electric springs," *IEEE Transactions on Smart Grid*, vol. 11, no. 5, pp. 3737-3747, Sept. 2020.

[34] Q. Wang, D. Zha, M. Cheng *et al*., "Energy management system for DC electric spring with parallel topology," *IEEE Transactions on Industry Applications*, vol. 56, no. 5, pp. 5385-5395, Sep. 2020.

[35] M. H. Wang, S. C. Tan, C. K. Lee *et al*., "A configuration of storage system for DC microgrids," *IEEE Transactions on Power Electronics*, vol. 33, no. 5, pp. 3722-3733, May 2018.

[36] H. Abdeltawab and Y. A. R. I. Mohamed, "Energy storage planning for profitability maximization by power trading and ancillary services participation," *IEEE Systems Journal*, vol. 16, no. 2, pp. 1909-1920, Jun. 2022.

[37] Q. Wang, S. Li, H. Ding *et al*., "Planning of DC electric spring with particle swarm optimization and elitist non-dominated sorting genetic algorithm," *CSEE Journal of Power and Energy Systems*, vol. 10, no. 2, pp. 574-583, Mar. 2024.

[38] D. Moeini and A. Chandra, "Coordinated energy-sharing Scheme for DC Electric Spring and Hybrid Battery Energy Storage Source in Modern DC Microgrids," in *Proceedings of 2022 IEEE Electrical Power and Energy Conference*, Victoria, Canada, Dec. 2022, pp. 302-306.

[39] C. Guo, Y. Wang, J. Liao *et al*., "Coordinated control of distributed renewable energy in bipolar DC microgrid based on modulus transformation," *Energy Reports*, vol. 9, pp. 1807-1817, Dec. 2023.

[40] M. Yang, R. Zhang, N. Zhou *et al*., "Unbalanced voltage control of bipolar DC microgrid based on distributed cooperative control," in *Proceedings of 2020 15th IEEE Conference on Industrial Electronics and Applications*, Kristiansand, Norway, Nov. 2020, pp. 339-344.

Xuefei Zhang received the B.S. and M.S. degrees in electrical engineering from Kunming University of Science and Technology, Kunming, China, in 2018 and 2021, respectively. He is currently pursuing the Ph.D. degree in School of Electrical Engineering, Chongqing University, Chongqing, China. His research interests include modeling, optimization, and operation of power system.

Chunsheng Guo received the B.E. degree with the College of Electrical Engineering, Sichuan University, Chengdu, China, in 2017, and the M.Eng. degree with the Department of Electrical and Electronic Engineering, University of Nottingham, Nottingham, U.K., in 2018, both in electrical engineering. He is currently working toward the Ph.D. degree in electrical engineering with Sichuan University. His research interests include bipolar DC microgrid, voltage balancing and power system stability and control.

Yiyao Zhou received the B.S. degree from Chongqing University, Chongqing, China, in 2018, and the M.E. degree from Hefei University of Technology, Hefei, China, in 2021. He is currently pursuing the Ph.D. degree in School of Electrical Engineering, Chongqing University. His research interests include modeling, optimization, and operation of distribution network.

Xiaolong Xu received the B.S. degree in electrical engineering and automation from China University of Petroleum, Qingdao, China, in 2021, and he is currently pursuing the Ph.D. degree with the School of Electrical Engineering, Chongqing University, Chongqing, China. His research interests include voltage stability of distribution networks.

Jianquan Liao received the B. S. degree in electrical engineering from China University of Petroleum, Qingdao, China, in 2017, and the Ph.D. degree from Chongqing University, Chongqing, China, in 2021. From September 2019 to September 2020, he was a Guest Researcher with Delft University of Technology, Delft, The Netherlands, where he was with DC Systems, Energy Conversion and Storage Group in Electrical Sustainable Energy. He has been an Associate Research Fellow with the School of Electrical Engineering, Sichuan University, Chengdu, China, since 2021. His current research interests include power system protection and control, power quality of DC distribution network, and power system stability and control.

Niancheng Zhou received the B.S., M.S., and Ph.D. degrees in electrical engineering from Chongqing University, Chongqing, China, in 1991, 1994, and 1997, respectively. He worked at Chongqing Kuayue Technology Co., Ltd., Chongqing, China, from 1997 to 2003. From 2010 to 2011, he was a Research Fellow of Nanyang Technological University, Singapore. He is a Professor in School of Electrical Engineering, Chongqing University. His research interests include analysis and operation of power system, microgrid, and power quality.

Qianggang Wang received the B. S. and Ph. D. degrees from Chongqing University, Chongqing, China, in 2009 and 2015, respectively. He was a Research Fellow with Nanyang Technological University, Singapore, from 2015 to 2016. He is currently an Associate Professor with the School of Electrical Engineering, Chongqing University. His research interests include analysis and operation of power system, microgrid, and power quality.